ELSEVIER

PII:S0263-8223(96)00035-9

Composite Structures 35 (1996) 271-281

0263-8223/96/$15.00

Multiobjective material architecture optimization of pultruded FRP I-beams

Julio F. Davalos, Pizhong Qiao

Department of Civil and Environmental Engineering, Constructed Facilities Center, West Virginia University, Morgantown, WV 26506-6103, USA

&

Ever J. Barbero

Department of Mechanical and Aerospace Engineering, Constructed Facilities Center, West Virginia University, Morgantown, WV 26506-6103, USA

This paper presents the application of micro/macromechanics models and optimization techniques for the optimum design of pultruded glass fiber-reinforced plastic composite I-beams with respect to material architecture: fiber orientations and fiber percentages. The beams are subjected to transverse loading, and beam deflection, buckling resistance and material failure are considered as multiple objectives (criteria) in the optimization process. Assuming a symmetrical laminated structure for the pultruded sections, experimentally verified micro/macromechanics models are used to predict ply properties, beam member response and ply strains and stresses. The Tsai–Hill failure criterion is used to determine first-ply-failure loads. Considering the coupling of lateral and distortional buckling, a stability Rayleigh–Ritz solution is used to evaluate the critical buckling loads for pultruded I-beams, and the results are verified with finite element analyses. A multiobjective design optimization formulation combined with a global approximation technique is proposed to optimize beam fiber architecture, which can greatly enhance the load carrying capacity of a section. The optimization procedure presented in this paper can serve as a practical tool to improve the performance of existing fiber-reinforced plastic without changing the current geometries. Copyright © 1996 Elsevier Science Ltd.

1 INTRODUCTION

Composite materials offer the advantage of tailoring the constituents for specific applications. This advantageous characteristic of composites can be realized fully by designing the material architecture to overcome controlling constraints, such as deflection, material failure and elastic buckling. The structural properties of pultruded fiber-reinforced plastic (FRP) shapes, including stiffness, strength and buckling resistance, depend on the material system (lay-up) and the cross-sectional geometry (shape) of the members.[1] For existing pultruded FRP shapes, we can optimize the material architecture by selectively specifying materials from a variety of resins, fiber systems, ply fiber orientations and ply fiber percentages, which can be designed to produce a desired optimum behavior. FRP shapes are commonly fabricated using fiberglass and either polyester or vinylester resins. Due to the low modulus of elasticity of glass fibers and the common thin-walled sectional geometry, pultruded FRP beams are susceptible to large deflections and buckling under service loads. In addition, due to the low shear ply strengths, material failure is also an important design parameter for beams subjected to transverse loads. For existing FRP shapes, the optimization of material architecture can significantly improve their loading capacities, with minor cost increases and modifications of existing processing limitations.

Unlike the extensive works reported for the optimal design of laminated composite plates and shells,[2,3] the material architecture and shape optimization of thin-walled laminated composites beams is still under investigation and is less developed. Morton and Webber[4] developed a procedure for obtaining an optimal design of a constant-section composite I-beam. By using a cyclic design-and-test strategy combined with heuristic redesign rules and a complex method, they obtained an optimal solution in terms of a set of cross-sectional dimensions. Qiao *et al.*[5] proposed an optimization method to minimize the cross-sectional area for new pultruded FRP beams. The beam members were subjected to transverse loading, and the optimization constraints included deflection limit, material failure and elastic buckling. A global approximation technique was combined with a power law to generate the constraint equations at a number of design points. Davalos *et al.*[6] improved the above work and presented a design and optimization approach for structural composite beams. An optimized winged-box section was proposed as a new structural shape with significantly better performance than a counterpart I-beam of the same cross-sectional area.

In this paper, a multiobjective (multicriteria) design optimization of material architecture (ply fiber orientations and ply fiber percentages) for pultruded FRP shapes is presented. Based on an experimentally verified micro/macromechanics formulation, a practical design tool for analyzing the performance (flexural behavior, buckling response and material failure) of FRP shapes is proposed. A wide flange I-section beam, which is one of the most commonly used structural shapes, is chosen to illustrate the analysis and design optimization. The beam maximum deflection, buckling resistance and material failure are considered as multiple objectives (criteria) in the optimization process. The optimal solutions are obtained through a multiobjective scheme, and a recommended practical design is proposed which is used to manufacture and test an actual section. The analytical tools presented in this paper are used to evaluate the test sample, and the results are discussed briefly.

2 CHARACTERIZATION OF PLY MATERIALS

The modeling of FRP shapes requires several material properties, but primarily longitudinal and transverse moduli and strengths and in-plane shear stiffness and strength for each ply (layer) of each panel of the cross-section. These properties need to be predicted during the design and optimization process. Most pultruded FRP sections, such as wide-flange and box shapes, consist typically of arrangements of flat walls or panels. Usually, the reinforcement used is E-glass fibers, and the resin matrix is either vinylester or polyester. Although pultruded FRP shapes are not laminated structures in a rigorous sense, they are pultruded with material architectures that can be simulated as laminated configurations.[1] A typical pultruded section may include the following four types of layers:[7] (1) a thin layer of randomly oriented chopped fibers (Nexus) placed on the surface of the composite. This is a resin-rich layer primarily used as a protective coating, and its contribution to the laminate response can be neglected; (2) continuous strand mats (CSM) of different weights consisting of continuous randomly oriented fibers; (3) stitched fabrics (SF) with different angle orientations; and (4) roving layers that contain continuous unidirectional fiber bundles, which contribute the most to the stiffness and strength of a section. Each layer is modeled as a homogeneous, linearly elastic and generally orthotropic material.

In this study, we optimize the material architecture of a commercially available I-section shape ($304{\cdot}8\times304{\cdot}8\times12{\cdot}7$ mm ($12\times12\times1/2$ inches)), consisting of E-glass fibers and vinylester matrix (Fig. 1). The material properties of the constituents (E-glass fiber and vinylester matrix) are considered to be isotropic.[7] The material architecture of the web and flanges includes sets of CSM, angle-ply SF and rovings (unidirectional fibers) arranged through the thickness of each panel. The symmetric lay-up consists of an idealized $(3n-1)$ number of layers with n CSM layers, n SF layers and $(n-1)$ roving layers, as shown in Fig. 1. The idealized layer thicknesses of SF and CSM layers (t_{SF} and t_{CSM}) and their corresponding fiber volume fractions ($(V_f)_{SF}$ and $(V_f)_{CSM}$) are evaluated using the information provided by the material producer and pultrusion manufacturer (see Davalos *et al.*[7]). The total thickness of a panel, t (web or flange), is designed as

$$t=nt_{SF}+n_{CSM}+(n-1)t_r \qquad (1)$$

where for a given panel thickness and t_{SF} and t_{CSM} thicknesses, the roving layer thickness, t_r,

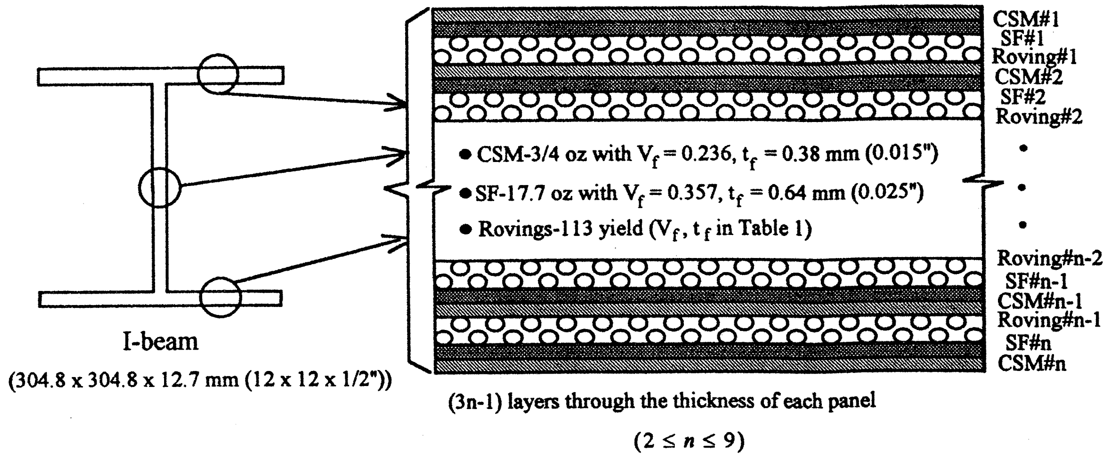

Fig. 1. Simulation of idealized lay-up system for pultruded FRP I-beam.

can be computed from eqn (1). Similarly, the fiber volume fraction of a panel, V_f, is expressed as

$$V_f=\frac{n(V_f)_{SF}t_{SF}+n(V_f)_{CSM}t_{CSM}+(n-1)(V_f)_r t_r}{t} \tag{2}$$

where $(V_f)_r$ is the fiber volume fraction of the roving layer. For a roving layer, $(V_f)_r$ can be independently computed by knowing t_r, the number of rovings per unit width (given by the manufacturer), and the yield density (given by the material supplier) (see Davalos *et al.*[7]).

Considering practical limitations of the pultrusion process, the following constraints are observed in the material design optimization: (1) the fiber volume fraction, V_f, or total percentage of fiber, X_f, of the section does not exceed 45% (V_f(or X_f)$\le$45%); and (2) the ply materials used are specified as 3/4 oz CSM, 17·7 oz SF and 113 yield (yard/lb.) roving, which are commercially available and commonly used in pultruded FRPs. The layer thicknesses, t_{CSM} and t_{SF}, are available from the material suppliers, and fiber volume fractions for $(V_f)_{CSM}$ and $(V_f)_{SF}$ are obtained following Davalos *et al.*[7] The fiber percentages of SF, CSM and roving layers in a panel, or equivalently the whole section, can be defined as

$$X_{CSM}=\frac{n(V_f)_{CSM}t_{CSM}}{t}\times 100\%$$

$$X_{SF}=\frac{n(V_f)_{SF}t_{SF}}{t}\times 100\%$$

$$X_r=\frac{(n-1)(V_f)_r t_r}{t}\times 100\% \tag{3}$$

Using the materials and limitations described above, the fiber percentages are given in Table 1. Note that $(V_f)_r$ is given relative to t_r, whereas X_r is the fiber percentage of roving relative to the section.

In this study, the design variables are the fiber percentages of SF, CSM and roving layers in the section (Table 1), and the fiber orientations of the SF layers (θ_{SF}). Considering current manufacturing practices, the following upper and lower bounds are imposed on the design variables:

$$0°\le\theta_{SF}\le 90°$$

$$3{\cdot}7\%\le X_{SF}\le 16{\cdot}7\%$$

$$1{\cdot}4\%\le X_{CSM}\le 6{\cdot}4\%$$

$$21{\cdot}9\%\le X_r\le 39{\cdot}9\% \tag{4}$$

For pultruded sections, it is not practical to evaluate the ply stiffnesses through experimental tests, since the material is not produced

Table 1. Lay-up design and fiber percentages in I-section

n	t_r (mm)	$(V_f)_r$	X_{SF} (%)	X_{CSM} (%)	X_r (%)
2	10·617	0·477	3·7	1·4	39·9
3	4·801	0·495	5·6	2·1	37·3
4	2·845	0·517	7·4	2·8	34·7
5	1·880	0·545	9·3	3·5	32·2
6	1·295	0·583	11·1	4·2	29·6
7	0·914	0·635	13·0	5·0	27·0
8	0·635	0·712	14·9	5·7	24·5
9	0·406	0·837	16·7	6·4	21·9

Table 2. Engineering constants of layers in I-section

Layer	V_f	E_1 (GPa)	E_2 (GPa)	G_{12} (GPa)	υ_{12}	$X^*_{T/C}$ (MPa)	$Y^*_{T/C}$ (MPa)	S^* (MPa)
3/4 oz/CSM	0·236	11·989	11·989	4·290	0·398	145·854	58·150	28·958
113 yield roving	0·635	47·220	16·027	5·875	0·322	661·297	58·150	28·958
17·7 oz $\pm\theta°$ SF	0·357	28·481	8·744	3·136	0·339	661·297	58·150	28·958

$^*X_{T/C}$, $Y_{T/C}$=longitudinal and transverse strengths in tension/compression; S=shear strength.

by lamination lay-up. Instead, the ply stiffnesses can be predicted by several formulas of micromechanics of composites.[7] In this study, the ply stiffnesses in Table 2 are computed from a micromechanics model for composites with periodic microstructure,[8] which, in combination with macromechanics,[9] have been shown to correlate well with experimental results for coupon samples.[10] Since ply strength values cannot be accurately predicted by standard micromechanics models developed for aerospace-type composites, a set of approximate micromechanics models for FRPs, sometimes including empirical correction factors, have been developed and correlated with experimental data.[11–13] In this study, we predict first-ply-failure (FPF) based on the ply strengths shown in Table 2, which were evaluated from existing proposed models.

3 ANALYSIS OF PULTRUDED FRP BEAMS

Because of the complexity of composite materials, analytical and design tools developed for members of conventional materials cannot always be readily applied to FRP shapes, and numerical methods, such as finite elements, are often difficult and expensive to use and require specialized training. Therefore, to expand the structural applications of pultruded FRP sections and create a new family of efficient FRP shapes for civil engineering structures, a comprehensive engineering analysis and design tool for pultruded FRP shapes has been developed. The analyses of FRP beams for elastic, failure and buckling responses are discussed next.

3.1 Deflection predictions

In this study, the response of FRP shapes in bending is evaluated using the mechanics of thin-walled laminated beams (MLB),[14] a formal engineering approach based on kinematic assumptions consistent with Timoshenko beam theory. MLB can be applied to FRP stuctural shapes with either open or closed cross-sections consisting of assemblies of flat walls; it is suitable for straight FRP beam–columns with at least one axis of geometric symmetry. For each laminated wall (e.g. a flange or a web), characterized by a local contour coordinate s_i and an angle ϕ_i (as shown in Fig. 2 for an I-section), the compliance matrices $[\alpha]_{3\times3}$, $[\beta]_{3\times3}$, $[\delta]_{3\times3}$, are obtained from classical lamination theory (CLT).[9] Incorporating stress resultant assumptions compatible with beam theory without torsion and assuming that the off-axis plies are balanced symmetric ($\alpha_{16}=\beta_{16}=0$), the extensional, bending–extension coupling, bending and shear stiffnesses of each panel are expressed as:

$$\begin{aligned}&\bar{A}_i=(\delta_{11}\Delta^{-1})_i,\\ &\bar{B}_i=(-\beta_{11}\Delta^{-1})i,\ \bar{D}_i=(\alpha_{11}\Delta^{-1})_i\\ &\bar{F}_i=(\alpha_{66}^{-1})_i\end{aligned} \tag{5}$$

where $\Delta=\alpha_{11}\delta_{11}-\beta_{11}^2$. General expressions for the beam stiffness coefficients are derived from the beam variational problem. Hence, axial (A_z), bending–extension coupling (B_x or B_y), bending (D_x or D_y) and shear (F_x or F_y) stiffnesses that account for the contribution of all the wall panels can be computed as:

$$\begin{aligned}&A_z=\sum_{i=1}^{n}\bar{A}_ib_i\\ &B_y=\sum_{i=1}^{n}[\bar{A}_i(\bar{y}_i-y_n)+\bar{B}_i\cos\phi_i]b_i\\ &D_y=\sum_{i=1}^{n}\left[\bar{A}_i\left((\bar{y}_i-y_n)^2+\frac{b_i^2}{12}\sin^2\phi_i\right)\right.\\ &\qquad\left.+2\bar{B}_i(\bar{y}_i-y_n)\cos\phi_i+\bar{D}_i\cos^2\phi_i\right]b_i\\ &F_y=\sum_{i=1}^{n}\bar{F}_ib_i\sin^2\phi_i\end{aligned} \tag{6}$$

The beam bending–extension coupling coefficients (B_x or B_y) can be eliminated by defining the location of the neutral axis of bending (x_n or y_n). An explicit expression for the static shear correction factor (K_x or K_y) is derived from energy equivalence, and the location of the shear center is defined in order to decouple bending and torsion. Displacement and rotation functions can be obtained by solving Timoshenko's beam theory equilibrium equations. In particular, general expressions for maximum bending and shear deflections available in manuals can be used. For example, the maximum deflection for a three-point loading of a beam of span L and load P is (Fig. 2):

$$\delta=\delta_b+\delta_s=\frac{PL^3}{48D_y}+\frac{PL}{4K_yF_y} \tag{7}$$

3.2 Prediction of ply strains and stresses

For a beam loaded in the z–y plane, the axial, shear and bending stress resultants are N_z, V_y and M_y. Then, the strains and curvature at the middle surface of the ith wall are expressed as

$$\bar{\varepsilon}_z(s_i,z)=\frac{N_z}{A_z}+(y(s_i)-y_n)\frac{M_y}{D_y}$$

$$\bar{\gamma}_{sz}(s_i,z)=\frac{V_y}{K_yF_y}\sin\phi_i$$

$$\bar{\chi}_z(s_i,z)=\frac{M_y}{D_y}\cos\phi_i \tag{8}$$

and the stress resultants in the ith wall are

$$\bar{N}_z(s_i,z)=\bar{A}_i\bar{\varepsilon}_z+\bar{B}_i\bar{\chi}_z,\quad \bar{N}_{sz}(s_i,z)=\bar{F}_i\bar{\gamma}_{sz}$$
$$\bar{M}_z(s_i,z)=\bar{B}_i\bar{\varepsilon}_z+\bar{D}_i\bar{\chi}_z \tag{9}$$

Ply strains and stresses, at a location (s_i,z) of the ith wall, can be obtained from classical lamination theory (CLT)[9] using the stress resultants given in eqn (9).

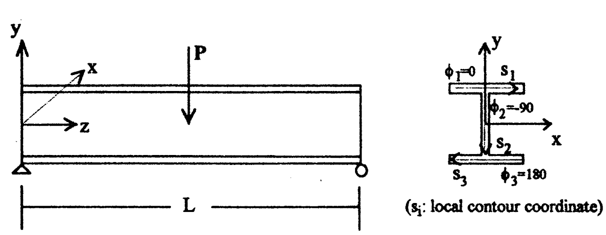

Fig. 2. Beam loading condition and reference coordinate systems.

3.3 First-ply failure

The Tsai–Hill failure criterion is used to predict the first-ply-failure (FPF) mid-span load (P_{FPF}) as

$$\frac{P}{P_{\text{FPF}}}=\sqrt{\left[\left(\frac{\sigma_1}{X}\right)^2+\left(\frac{\sigma_2}{Y}\right)^2-\frac{\sigma_1\sigma_2}{X^2}+\left(\frac{\tau_{12}}{S}\right)^2\right]} \tag{10}$$

where σ_1, σ_2 and τ_{12} are the components of in-plane ply-stresses in material coordinates, and X, Y and S are the corresponding ply strengths.

3.4 Lateral-torsional and distortional buckling of pultruded FRP I-beams

Pultruded FRP I-beams are susceptible to lateral and distortional buckling. A few studies on the combined analysis of lateral-torsional and local buckling modes of I-beams have been presented,[15,16] based on an energy approach to detect instability.

In this study, we use the formulation presented by Barbero and Raftoyiannis[16] to evaluate the lateral-torsional and distortional buckling response of FRP I-beams. The coupling of lateral and local buckling for pultruded I-beams is considered. In the adopted formulation, the von Karman nonlinear strain–displacement relations are used to describe the deformation of the web panel, while the displacements of the flange panels are assumed to be linear in the coordinate s_i; however, the flanges can bend and twist as plates and also bend laterally as beams. The equilibrium equation in terms of the total potential energy is solved by the Rayleigh–Ritz method. For the web, the following displacement function is selected

$$\delta w=\sum_{m=1}^{p}\sum_{n=1}^{q}\alpha_{mn}\sin\left(\frac{m\pi z}{a}\right)\left(\frac{y}{b}\right)^n \tag{11}$$

where the coordinates z and y are defined in Fig. 2, and p and q defined the desired order of approximation. By selecting the values of p and q, we can define the buckle shapes and determine the corresponding critical distortional buckling loads. For further details see the original reference.[16]

3.5 FRPBEAM computer program

Based on the modeling assumption and analytical tools for FRP beams discussed previously, the computer program FRPBEAM (flowchart shown in Fig. 3) was developed by Qiao *et al.*[17] to model, analyze and design FRP beams, from the evaluation of ply stiffnesses by micromechanics to the overall beam response by MLB and buckling analysis by the Rayleigh–Ritz method. The MLB subroutine can accurately predict displacements and strains of pultruded FRP beams.[7,10] The Rayleigh–Ritz method is used as a subroutine for solving eigenvalue problems and predicting critical buckling loads and modes for FRP I-beams. To verify the accuracy of the FRPBEAM program for buckling prediction, the pultruded FRP I-beam of Fig. 2 is also analyzed with the commercial finite element program ANSYS[18] using eight-node isoparametric layered shell elements (SHELL 99), which include shear deformation. The buckling load predictions with the FRPBEAM program match closely those given by the finite element solution, as shown in Fig. 4 for the optimized section discussed later in this paper.

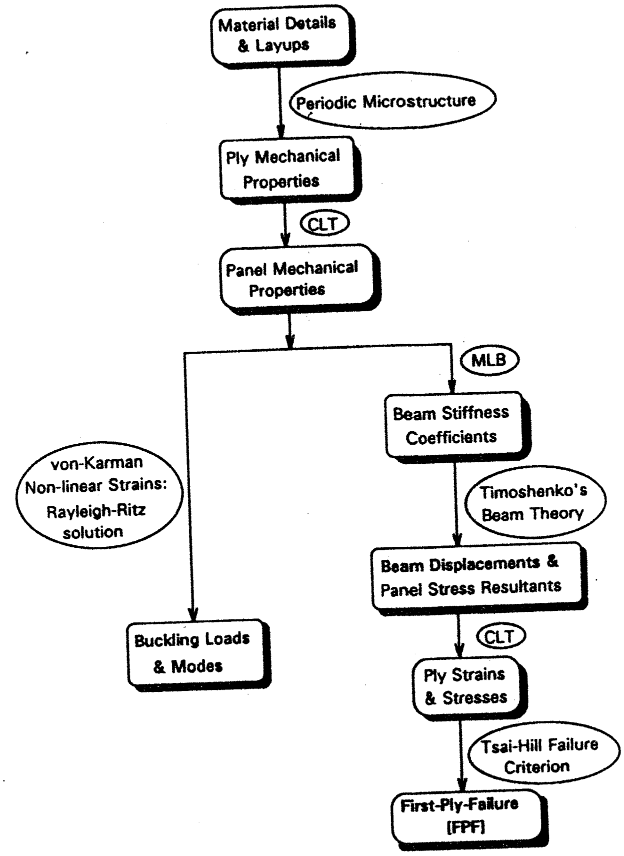

Fig. 3. Computational flowchart of FRPBEAM program.

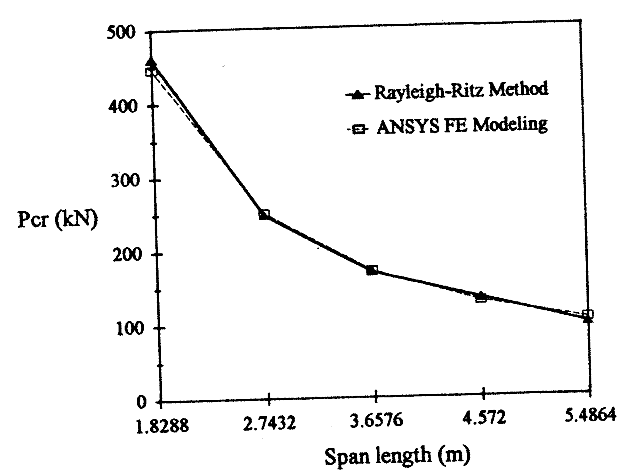

Fig. 4. Critical buckling loads for optimized 'as manufactured' FRP I-beam.

4 MULTIOBJECTIVE OPTIMIZATION OF MATERIAL ARCHITECTURE

As previously explained, transverse deflection and buckling resistance are important considerations in design of pultruded FRP beams. On the other hand, material failure can govern the design of short- and intermediate-span beams under transverse shear loads. The design of material architecture of pultruded FRP beams is a multicriteria task and may be best accomplished as a constrained optimization of multiple objective functions.

4.1 Scheme of multiobjective optimization formulation

In this study, a global criterion method (min–max formulation)[19] involving minimization of multiple objective functions is applied to solve the optimization problem. In this method an optimal vector is found by minimizing some global criterion, such as the sum of the squares of the relative deviation of the criteria from the feasible ideal points. The problem is defined as a constrained multiobjective problem involving minimization (or maximization) of k objective functions

$$\min f_j(\mathbf{x}), \quad j=1,2,\ldots,k \tag{12}$$

subject to m equality (or inequality) constraints $g_i(\mathbf{x})$ and lower and upper bounds on the design vector $\mathbf{x}$

$$g_i(\mathbf{x}) \leq 0, \quad i=1,2,\ldots,m \tag{13}$$

$$\mathbf{x}^{\mathrm{L}} \leq \mathbf{x} \leq \mathbf{x}^{\mathrm{U}} \tag{14}$$

By minimizing individual objective functions subject to constraints given in eqns (13) and (14), we could obtain the feasible ideal solution $f_j(\mathbf{x}^*)$ for each objective. These ideal solutions define a target point $f_j(\mathbf{x}^*)$ in the design domain. Then the method of global criterion for solving the vector minimum problem is given by

$$\min \sum_{j=1}^{k} \left(\frac{f_j(\mathbf{x}) - f_j(\mathbf{x}^*)}{f_j(\mathbf{x}^*)} \right)^p \tag{15}$$

subjected to constraints of eqns (13) and (14); where p is generally taken as 2 (Euclidean metric). In this study, the multiple objective functions in eqn (12) represent the deflection (δ), buckling load function ($1/P_{\mathrm{cr}}$) and material failure load function ($1/P_{\mathrm{PFP}}$), and the constraints in eqn (14) are the bounds on the design variables as defined in eqn (4). There are no inequality constraints in the optimization process. A four-stage multiobjective optimization scheme used in this study is illustrated in Fig. 5. The minimization of individual objective functions and global criterion function can be accomplished with available constrained optimization algorithms. However, the evaluation of functions for the deflections, buckling loads and material failure loads can be a difficult problem and a time-consuming effort involving explicit and/or numerical analyses to define their design space. In this study, the functions for deflections, critical buckling loads and FPF loads are

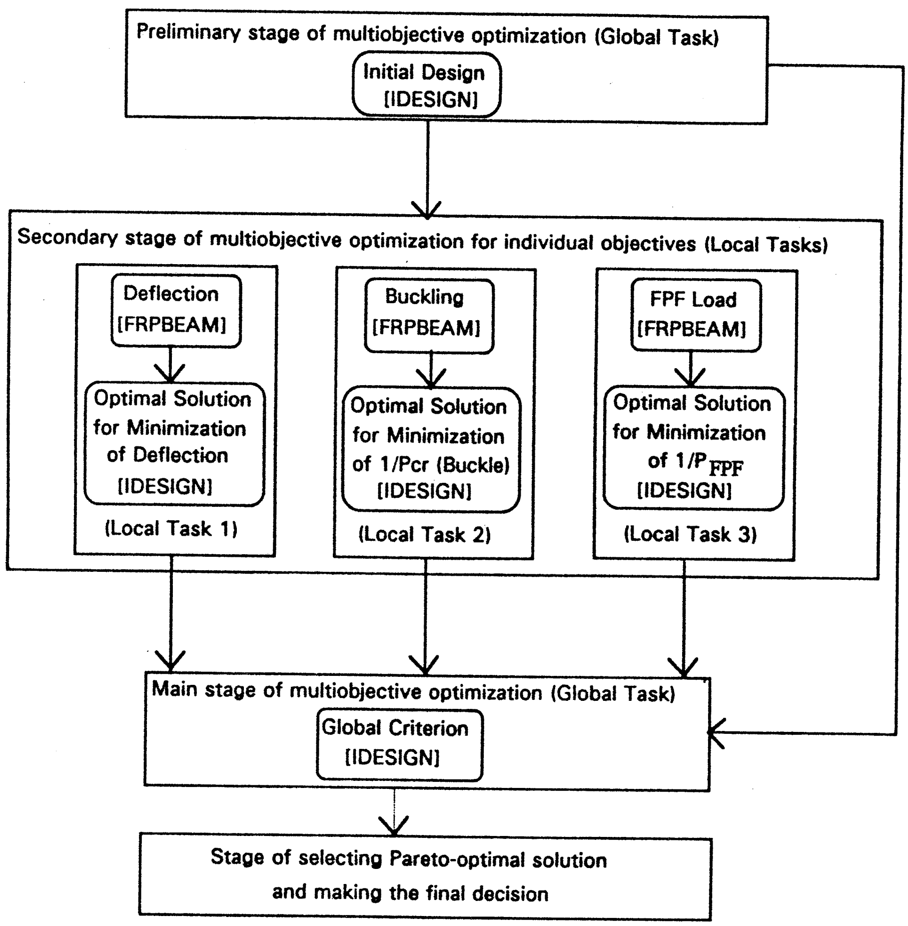

Fig. 5. Four-stage multiobjective optimization scheme.

generated through global approximations.[2] The functions are evaluated at a number of design points using the FRPBEAM program (Fig. 3) and are expressed in terms of the design variables using regression analysis models.[5] Statistical measures are used to assess the goodness-of-fit, or the accuracy, of the numerical fittings of predicted functions, and a normalization on design variables is implemented to minimize round-off errors in the optimization process.

4.2 Optimal design of FRP I-beam material architecture

The optimal design problem is concerned with simply supported beams under a mid-span concentrated load. Two span lengths of 1·829 m (6 ft) and 3·658 m (12 ft) are considered in the analyses. A four-stage optimal design process (Fig. 5) is carried out for each span. The first (preliminary) stage is concerned with the initial design of material architecture, as presented in Section 2. In the second stage, we analyze the beams with various material architectures using the FRPBEAM program, and the prediction functions for deflection, buckling load ($1/P_{cr}$) and first-ply-failure load ($1/P_{FPF}$) are generated by using regression models. We optimize the material architecture (fiber percentages and fiber orientations) with respect to each single objective function, and local optimal solutions are obtained. Thus, at this secondary stage, all local tasks are defined with respect to their single objectives and constitute independent simulations. Then in the third (main) stage, the global criterion defined in eqn (15) is used to carry out the multiobjective optimization task, which includes the contributions of all three local objectives in a global sense. In the final stage, the Pareto-optimal solution[19] is selected, and a final decision is made on the optimal material architecture. At every stage, the optimization scheme is used in conjunction with the commercial program IDESIGN,[20] to obtain the optimal solution for the local and global tasks.

5 NUMERICAL RESULTS AND DISCUSSIONS

Using the design scheme and optimization techniques presented earlier, we carry out the analyses and optimal design of a pultruded FRP I-beam of given cross-section (304·8 × 304·8 × 12·7 mm (12 × 12 × ½ inches)). For a span $L = 3{\cdot}658$ (12·0 ft), the influence of fiber orientation (θ_{SF}) and fiber percentage (X_f) of SF on deflections, buckling loads and FPF loads are shown, respectively, in Figs 6–8. Tables 3 and 4 show the results for span-lengths of 1·829 m (6·0 ft) and 3·658 m (12·0 ft), respectively. The results show the optimal material architectures for each individual objective functions and also for the global multiobjective function. When an individual objective is optimized, the best result is obtained for the criterion considered, whereas the multiobjective optimization pro-

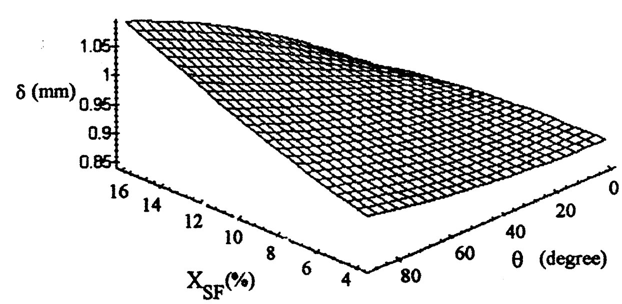

Fig. 6. Influence of fiber orientations (θ) and fiber percentages (X_{SF}) of SF on deflection (δ).

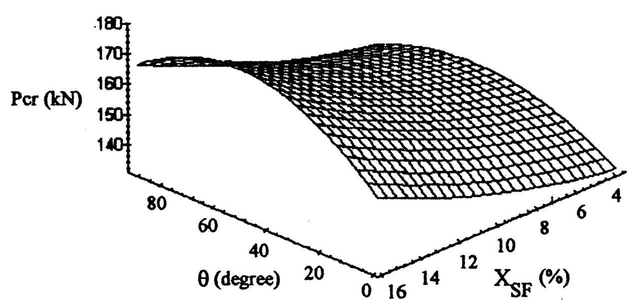

Fig. 7. Influence of fiber orientations (θ) and fiber percentages (X_{SF}) of SF on buckling resistance (P_{cr}).

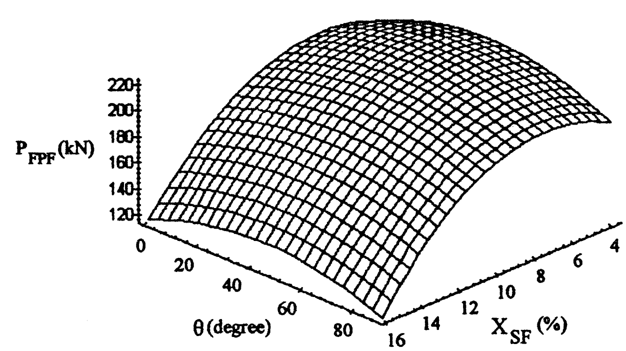

Fig. 8. Influence of fiber orientations (θ) and fiber percentages (X_{SF}) of SF on first-ply-failure load (P_{FPF}).

vides a design accounting simultaneously for all three criteria. Consistent with the specified constraint, the total fiber percentage (X_f) for the section is around 45% for any design (i.e. $X_{SF}+X_{CSM}+X_r \leq 45\%$). The orientations of SF layers vary among the invididual optimization objectives, but for the multiobjective design, the average is about 45°. The multiobjective design combines the attributes of minimum deflection, maximum buckling load and maximum FPF load designs and exhibits the best characteristics for structural performance. The optimizations with single-objective functions show a strong tendency to overdesign the structure for one criterion, without improving all objectives simultaneously.

Table 3. Optimum design results for $L=1{\cdot}829$ m (6·0 ft)

Result	Min ($1/P_{cr}$)	Min (δ)	Min ($1/P_{FPF}$)	Multi-objective design
X_{SF} (%)	16·7	16·7	7·840	10·85
X_{CSM} (%)	6·4	6·4	2·967	4·11
X_r (%)	21·9	21·9	34·194	30·045
$\theta°$ in SF	62·1°	20·2°	29·9°	41·8°
P_{cr} (kN)	499·419	463·949	397·822	429·195
δ (mm)	0·187	0·174	0·193	0·178
P_{FPF} (kN)	130·769	126·321	242·459	233·696

Table 4. Optimum design results for $L=3{\cdot}658$ m (12·0 ft)

Result	Min ($1/P_{cr}$)	Min (δ)	Min ($1/P_{FPF}$)	Multi-objective design
X_{SF} (%)	16·7	3·7	6·978	9·334
X_{CSM} (%)	6·4	1·4	2·64	3·513
X_r (%)	21·9	39·9	35·382	32·143
$\theta°$ in SF	50·0°	0·0°	42·8°	47·3°
P_{cr} (kN)	182·159	139·225	151·893	157·725
δ (mm)	1·008	0·887	0·904	0·927
P_{FPF} (kN)	122·001	190·540	229·831	215·481

Using the results of the multiobjective design, a practical material architecture is designed by considering the properties of existing available materials for CSM, SF and rovings. The recommended fiber architectures and corresponding section performances for practical designs are given in Table 5. In Table 1, the recommended fiber architectures consist of 17 layers (or $n=6$ in Fig. 1) for a 1·829 m (6·0 ft) span (six 17·7 oz SFs, six 3/4 oz CSMs and five 113-yield roving layers), and 14 layers (or $n=5$ in Fig. 1) for a 3·658 m (12·0 ft) span (five 17·7 oz SFs, five 3/4 oz CSMs and four 113-yield roving layers). The buckling loads for the two beam spans are obtained accounting for the combined effects of lateral-torsional and local buckling modes (distortional buckling). The first-ply-failure for the 1·829 m (6·0 ft) span takes place in the roving layer of the web at the junction with the top flange; whereas for the 3·658 m (12·0 ft) span it takes place in the SF layer of the web at the junction with the top flange.

Based on the recommended designs, a section was produced by industry with some architecture modifications to accommodate processing limitations; the architecture and performance of the 'as manufactured' section are given in Table 5, and the lay-up is shown in Fig. 9. Compared with the manufactured design, the recommended (optimized) design for the 1·829 m (6·0 ft) span provides a better performance for buckling (6·6%), maximum deflection (10·0%) and FPF load (11·2%), and similarly for the 3·658 m (12·0 ft) span the improvement in performance is 4·7% for buckling, 3·7% for deflection and 10·1% for FPF load. The 'as manufactured' section was tested in bending under three-point (load at mid-span) and also four-point (load at exactly third points) loadings. In Table 6, the measured mid-span maximum deflections and strains compare well

Table 5. Comparison between practical and manufactured designs

Design	$L=1{\cdot}829$ m (6·0 ft)		$L=3{\cdot}658$ m (12·0 ft)	
	Practical design	As manufactured	Practical design	As manufactured
X_{SF} (%)	11·1	13·0	9·3	13·0
X_{CSM} (%)	4·2	4·96	3·5	4·96
X_r (%)	29·6	26·30	32·2	26·30
$\theta°$ in SF	45·0°	45·0°	45·0°	45·0°
P_{cr} (kN)	442·780	415·326	160·550	153·366
δ (mm)	0·185	0·208	0·932	0·968
P_{FPF} (kN)	246·431	221·624	227·749	206·851

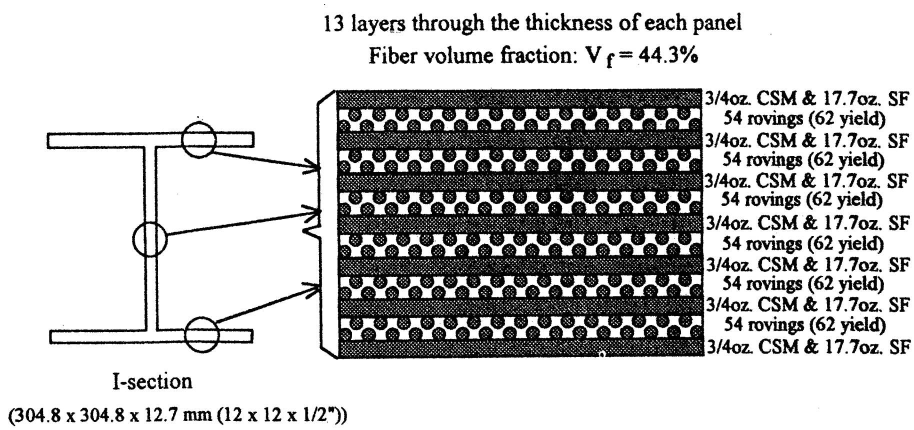

Fig. 9. Fiber architecture of 'as manufactured' FRP I-beam.

Table 6. Deflections and strains comparisons of 'as manufactured' beams

	$L = 1{\cdot}829$ (6·0 ft)				$L = 3{\cdot}658$ m (12·0 ft)			
	Three-point bending		Four-point bending		Three-point bending		Four-point bending	
	Experimental	FRPBEAM	Experimental	FRPBEAM	Experimental	FRPBEAM	Experimental	FRPBEAM
δ_{max} (mm/kN)	0·0504	0·0463	0·0388	0·0356	0·215	0·218	0·201	0·203
ε_{max} ($\mu\varepsilon$/kN)	13·630	14·096	9·578	9·465	23·897	25·628	18·165	18·794

with the predicted micro/macromechanics results (FRPBEAM program).[17]

6 CONCLUSIONS

In this paper, a multiobjective design optimization method for pultruded fiber-reinforced plastic (FRP) structural beams is presented. The design objectives include minimization of beam mid-span deflections and maximization of buckling loads and FPF loads. Micro/macromechanics models with an explicit stability solution and a failure criterion are integrated into a cohesive computer program for the analysis and design of pultruded FRP shapes. The computer program (FRPBEAM)[17] is an efficient tool to carry out the design and optimization process for an existing I-beam shape ($304{\cdot}8 \times 304{\cdot}8 \times 12{\cdot}7$ mm ($12 \times 12 \times 1/2$ in)), for which the fiber architecture is optimized. The optimizations for single-objective functions show a strong tendency to overdesign the material architecture for a single parameter (e.g. deflection), without improving all objectives simultaneously. The multiobjective optimal design algorithm blends and balances several merits of the individual single-objective optimizations and improves the beam performance in a global sense. The results presented in this paper indicate that without changing the current geometries, the performance of existing FRP shapes can be improved by using the present modeling methods and an innovative optimization technique, as proposed by the authors.

REFERENCES

1. Barbero, E. J., Pultruded structural shapes — from the constituents to the structural behavior. *SAMPE J.*, **27** (1) (1991) 25–30.
2. Haftka, R. T. & Gurdal, Z., *Elements of Structural Optimization*. Kluwer Academic, 1992.
3. Abrate, S., Optimal design of laminated plates and shells. *Composite Struct.*, **29** (1994) 269–86.
4. Morton, S. K. & Webber, J. P. H., Optimal design of a composite I-beam. *Composite Struct.*, **28** (1994) 149–68.
5. Qiao, P., Davalos, J. F. & Barbero, E. J., Optimal design of pultruded FRP shapes for structural applications. In *Proceedings of the 1st International Conference on Composites in Infrastructure (ICCI '96)*, Tucson, Arizona, eds H. Saadatmanesh & M. R. Ehsani, 1996, pp. 676–88.
6. Davalos, J. F., Qiao, P. & Salim, H. A., A practical design and optimization method for structural composite beams. In *Composites Institute's 51st Conference and EXPO '96, SPI, Cincinnati, Ohio*, 1996, pp. (24-D) 1–8.
7. Davalos, J. F., Salim, H. A., Qiao, P., Lopez-Anido, R. & Barbero, E. J., Analysis and design of pultruded

FRP shapes under bending. *Composites, Part B: Engng. J.*, **27B** (1996) 295–305.
8. Luciano, R. & Barbero, E. J., Formulas for the stiffness of composites with periodic microstructure. *Int. J. Solids Struct.*, **31** (1994) 2933–44.
9. Jones, R. M., *Mechanics of Composite Materials*. Hemisphere, New York, 1975.
10. Salim, H. A., Davalos, J. F., Qiao, P. & Barbero, E. J., Experimental and analytical evaluation of laminated composite box beams. *Proc. 40th Int. SAMPE Symp.*, **40** (1) (1995) 532–9.
11. Sonti, S. S., Stress analysis of pultruded structural shapes. Master thesis, West Virginia University, Morgantown, West Virginia, 1992.
12. Makkapati, S., Compressive strength of pultruded structural shapes. Master thesis, West Virginia University, Morgantown, West Virginia, 1994.
13. Tomblin, J. S., Compressive strength models for pultruded glass fiber reinforced composites. PhD dissertation, West Virginia University, Morgantown, West Virginia, 1994.
14. Barbero, E. J., Lopez-Anido, R. & Davalos, J. F., On the mechanics of thin-walled laminated composite beams. *J. Composite Mater.*, **27** (1993) 806–29.
15. Roberts, T. M. & Jhita, P. S., Lateral, local and distortional buckling of I-beams. *Thin-Walled Struct.*, **1** (1983) 289–308.
16. Barbero, E. J. & Raftoyiannis, I. G., Lateral and distortional buckling of pultruded I-beams. *Composite Struct.*, **27** (1994) 261–8.
17. Qiao, P., Davalos, J. F. & Barbero, E. J., FRPBEAM: a computer program for analysis and design of FRP beams. CFC-94-191, Constructed Facilities Center, West Virginia University, Morgantown, West Virginia, 1994.
18. *Users' Manual for ANSYS User*, Swanson Analysis Systems Inc., Houston, Pennsylvania, 1992.
19. Eschenauer, H., Koski, J. & Osyczka, A., *Multicriteria Design Optimization*. Springer, Berlin, 1990.
20. Arora, J. S., IDESIGN user's manual. Optimal Design Laboratory, The University of Iowa, Technical Report No. ODL-89.7, 1989.